Effects of Nucleon-Pair Correlations on Monte Carlo Intranuclear-Cascade Simulations*

K. Chen, G. Friedlander, G. D. Harp, and J. M. Miller
Chemistry Department, Brookhaven National Laboratory, Upton, New York 11973 and Columbia University, New York, New York 10027

(Received 15 July 1971)

The effects of short-range nucleon correlations have been included in intranuclear-cascade calculations in an approximate manner. Comparisons are made with earlier calculations and with experiments. The agreement with experimental data on spallation reactions and spectra of emitted protons is systematically improved when the nucleon-correlation effect is included, along with refraction and reflection at potential boundaries and with a velocity-dependent potential.

I. INTRODUCTION

Down through the years Monte Carlo intranuclear-cascade studies have become more sophisticated and, as a consequence, more complex.[1-5] Refinements in the nuclear models have sometimes, but not always, led to improved agreement with experimental data. A particularly puzzling result of calculations done with and without the refraction and reflection of cascade nucleons at the boundaries between regions of different potentials was that the latter (no-refraction) model gave better agreement with experimental results than did the former, physically more realistic model.[4] Further, the use of a velocity-dependent potential,[5] which also included the refraction and reflection of cascade nucleons, did not substantially improve the fits to the experimental data that were obtained from the previous "refraction-and-reflection" model. In the present paper, a possible reason for some of the shortcomings of these calculations is explored.

One nuclear property that has not previously been considered in these calculations is the correlation of nucleon positions in the target nucleus. To be more specific, consider the nucleon-pair-correlation function $G(\vec{r}, \vec{r}')$. As is well known, for an infinite isotropic system in which surface effects can be neglected, the spatial correlation between distinct particles depends only on $|\vec{r}-\vec{r}'|$ and may be discussed in terms of the radial distribution function which is familiar in both x-ray and neutron-diffraction studies and in the equilibrium statistical mechanics of dense fluids.[6]

$G(\vec{r}, \vec{r}')$ has the following basic properties:

(a) $\lim_{|\vec{r}-\vec{r}'|\to\infty} G(\vec{r}, \vec{r}') = 1.$

That is, nucleons become uncorrelated for large separations,

(b) $\int \rho(\vec{r}')G(\vec{r}, \vec{r}')d\vec{r}' = A-1$, where $\rho(\vec{r}')$ is the nucleon density at $\vec{r}'$ in a nucleus containing A nucleons. This normalization requirement for $G(\vec{r}, \vec{r}')$ is actually not very restrictive. For example, it is satisfied for $G(\vec{r}, \vec{r}')$ equal to $(A-1)/A$, which is the pair-correlation function for a noninteracting group of A Boltzmann particles.

The direct calculation of $G(\vec{r}, \vec{r}')$ is a many-body problem and hence very difficult. In approximate calculations of this function, two nuclear properties have to be considered: the Pauli exclusion principle and the potential of interaction between the nucleons. In infinite nuclear matter $G(\vec{r}, \vec{r}')$ is a function only of $|\vec{r}-\vec{r}'| = R$. Thus it is convenient to discuss nucleon correlations in such a system in terms of the radial distribution function $g(R)$. Because of the short-range character of nucleon-nucleon forces, the properties of $g(R)$ in infinite nuclear matter should also provide some information about nucleon spatial correlations in at least the inner regions of a finite nucleus.

Perhaps one of the most informative and instructive calculations of $g(R)$ was done by Moniz, Nixon, and Walecka,[7] who calculated the pair-correlation function for two interacting nucleons in an infinite nuclear medium. They assumed an internucleon potential that consisted of a hard-core repulsive potential at small distances and an exponential attractive potential at large distances. They also included the effect of the Pauli exclusion principle. Their distribution function displays the following features:

(1) $g(R) = 0$ for $R \lesssim 0.5$ F. This implies that given a particular nucleon, it is then impossible to find another nucleon within a sphere whose center corresponds to the center of the original nucleon and whose radius is ~0.5 F. This fact will be used later in an attempt to include the effects of nuclear correlations on intranuclear-cascade calculations.

(2) For $R > 0.5$ F, $g(R)$ first rises steeply from zero to ~0.75 for $0.5\ \text{F} < R \lesssim 1$ F and then much more gradually approaches its asymptotic value

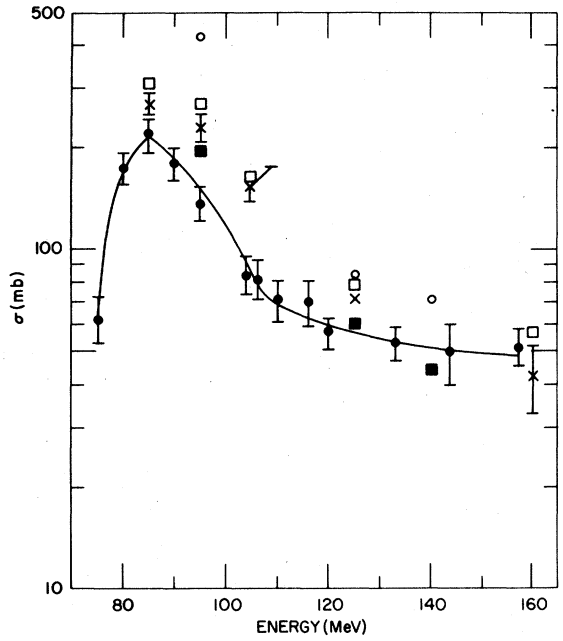

FIG. 1. Excitation function for the reaction ^{209}Bi$(p, 8n)$-^{202}Po. The solid points are the experimental data of Ref. 9. The open squares and crosses are calculated with the VPOT(0.5) and VPOT($V\rho = 1$) models, respectively. The open circles and solid squares are calculated with the STEP and STEPNO models, respectively. Since the statistical errors for the calculated cross sections are about the same for the different models, the errors for only a few representative points are given. The same is true for the rest of the figures which are presented.

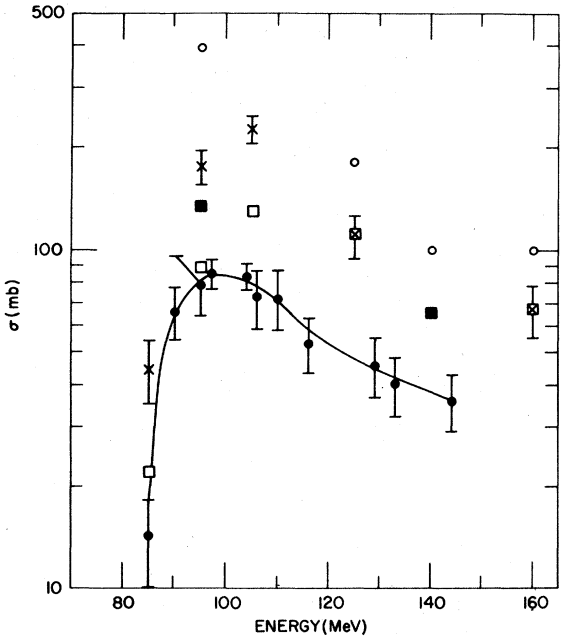

FIG. 2. Excitation function for the reaction ^{209}Bi$(p, 9n)$-^{201}Po. The symbols used have the same meaning as those used in Fig. 1.

of unity for $R > 1$ F.

Thus far, only some general properties of nuclear-correlation functions have been discussed. However, what is actually required is to include them, at least approximately, in intranuclear-cascade calculations. Therefore, in the following the reasons for their inclusion will be discussed and it will be shown that when they are included, even in an approximate manner, the agreement between experimentally determined properties of nuclear reactions and those predicted by intranuclear-cascade calculations is generally improved.

II. INCLUSION OF CORRELATION EFFECTS IN INTRANUCLEAR-CASCADE CALCULATIONS

Let us first discuss why correlations should be included in intranuclear-cascade calculations. In order to do so consider the details of a hypothetical cascade. Suppose the incident nucleon enters the nucleus and undergoes a Pauli-allowed collision at $\vec{r}_1$ with some nucleon in the target. Then suppose the incident and struck nucleon each make Pauli-allowed collisions with two other nucleons in the target at $\vec{r}_2$ and $\vec{r}_3$. The collision sites at $\vec{r}_1$, $\vec{r}_2$, and $\vec{r}_3$ represent the locations of three different target nucleons. Therefore, from our previous discussion of the nucleon-radial-distribution function, these sites must be separated by at least 0.5 F. However, since in previous intranuclear-cascade calculations[1-5] all cascade nucleons were treated as independent points, one can readily find, in examining such calculations,[4,5] cascades in which collision sites are separated by

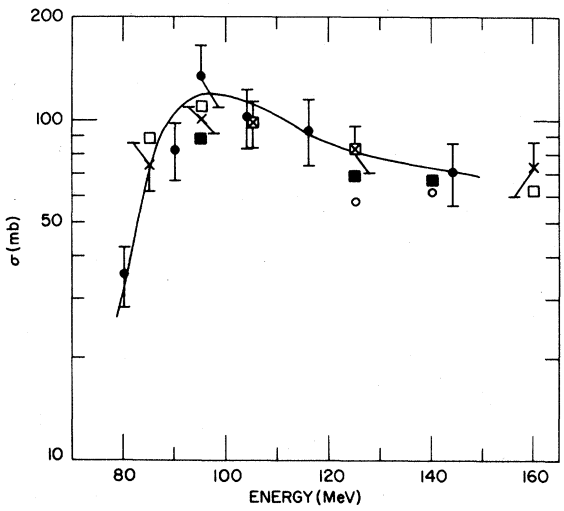

FIG. 3. Excitation function for the reaction ^{209}Bi$(p, p7n)$-^{202}Bi. The symbols used have the same meaning as those used in Fig. 1.

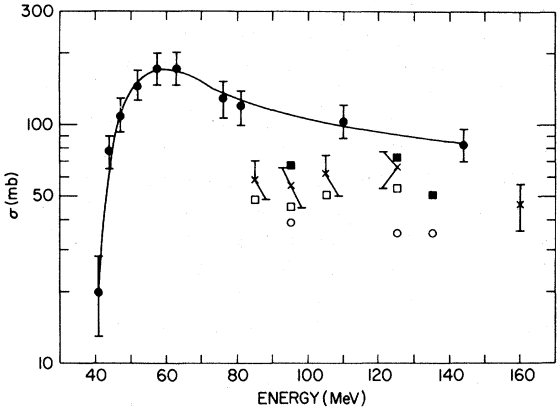

FIG. 4. Excitation function for the reaction ^{209}Bi$(p,p3n)$-^{206}Bi. The symbols used have the same meaning as those used in Fig. 1.

0.1 F or less. This is merely a reflection of the fact that in these cascade calculations short-range nucleon correlations in the target nuclei were completely neglected. As a consequence, one might expect these calculations to overestimate the number of nucleons involved in a cascade and thus the energy deposited in the target nucleus.

In order to circumvent the problems mentioned above, the short-range nucleon-correlation effect was approximated by simply imposing the restriction that if a given nucleon made a Pauli-allowed collision at the point $\vec{r}_1$, then neither the incident nor the struck nucleon were allowed to interact

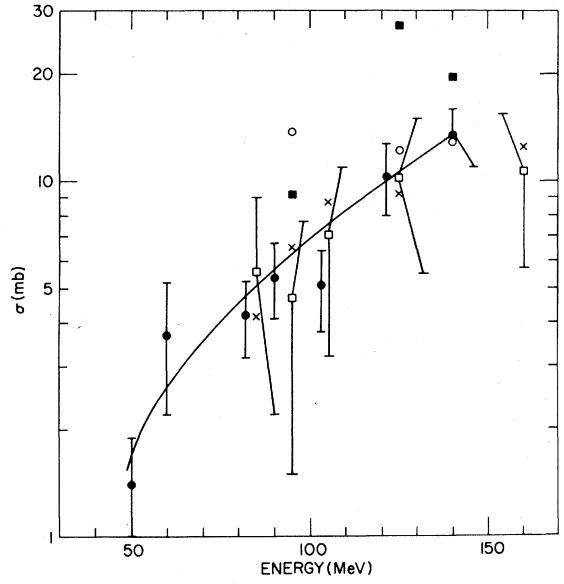

FIG. 5. Excitation function for the reaction ^{209}Bi$(p,2p6n)^{202}$Pb. The symbols used have the same meaning as those used in Fig. 1.

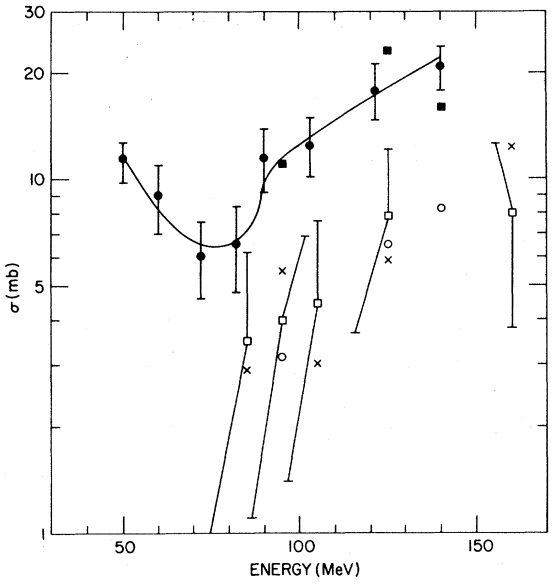

FIG. 6. Excitation function for the reaction ^{209}Bi$(p,2p5n)^{203}$Pb. The symbols used have the same meaning as those used in Fig. 1.

with another nucleon within a distance d from $\vec{r}_1$. Two values of d were used in the cascade calculations. The first and also the smallest value was 0.5 F which, from the previous discussion of the distribution function of Moniz, Nixon, and Walecka,[7] should be the minimum separation for two nucleons in a target nucleus. The second value of d that was used is density-dependent. If one simply assumes that each nucleon in a particular density region which is characterized by a total density ρ occupies the same volume V, then one has $V\rho = 1$. If one further assumes that a collision occurs in the center of the volume assigned

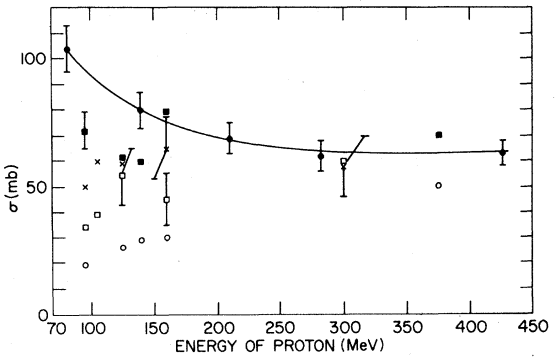

FIG. 7. Excitation function for the reaction ^{197}Au(p,pn)-^{196}Au. The solid points are the experimental data of Ref. 11. The open squares, crosses, open circles, and solid squares are calculated from the VPOT(0.5), VPOT($V\rho = 1$), STEP, and STEPNO models, respectively, for the reaction ^{209}Bi$(p,pn)^{208}$Bi.

to a particular nucleon, then one has the restrictive distance d simply given by $\frac{4}{3}\pi d^3\rho = 1$. In the following this restrictive distance will be denoted by $V\rho = 1$. Note that if one is dealing with a nucleus of constant density whose radius is $r_0 A^{1/3}$, then d is simply r_0, which is ~1.3 F.

Before proceeding further, let us briefly review some characteristics of the intranuclear-cascade models of Refs. 4 and 5. First, the nuclear-radial-density distribution was represented by a series of steps which approximated a Fermi distribution that was consistent with Hofstadter's data on the nuclear-charge distribution.[8] The step density distribution is equivalent to a series of concentric regions, each having a constant but different density. Each region was assigned a particular nuclear potential which acted on the cascade nucleons. Calculations were then done with and without the refraction and reflection of cascade nucleons as they moved from one potential region to another. One of the surprising and inexplicable results from these calculations was that for incident energies below 200 MeV, better agreement with experimental data was obtained if the refraction and reflection of cascade nucleons was neglected.[4]

Two possible explanations for this result were then proposed: (a) The classical treatment of refraction and reflection is such a poor approximation to a correct quantum mechanical treatment that it is better to ignore refraction and reflection entirely; (b) the potential used was incorrect. The first explanation was investigated and it was shown that just the converse was true.[4] The second explanation was partially explored by using a velocity-dependent potential of the form $V = V_0 \times (1 - \epsilon/\epsilon_{max})$ for $\epsilon < \epsilon_{max}$ and $V = 0$ for $\epsilon \geq \epsilon_{max}$, where ϵ is the kinetic energy of the cascade nucleon. This potential form was suggested by optical-model potential analyses of nucleon-nucleus scattering experiments which also suggest values of $\epsilon_{max} \gtrsim 100$ MeV. However, when cascade calculations were done using this potential, only slightly better agreement was obtained between the calculated and experimental results than was found previously using the velocity-independent potential.[5]

In the following the velocity-dependent potential will be used and some results of cascade calculations using this potential and the restrictive distances mentioned previously will be presented.

The objectives of this study are then: (1) to study the effects of short-range nucleon correlations, and (2) to see if these effects allow one to get satisfactory results when refraction and reflection are treated classically. For the sake of brevity, this cascade model will be denoted as VPOT(d) where d refers to the particular restrictive distance used, i.e., 0, 0.5 F, or $V\rho = 1$. Further, all calculations were done with ϵ_{max} = 100 MeV. Brief comparisons will be made with re-

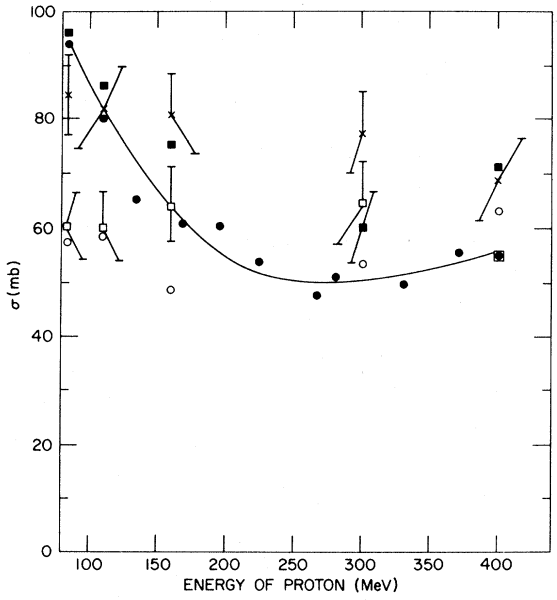

FIG. 8. Excitation function for the reaction ^{65}Cu(p,pn)-^{64}Cu. The solid points are the experimental data of Ref. 12. The open squares, crosses, open circles, and solid squares are calculated with the VPOT(0.5), VPOT($V\rho = 1$), STEP, and STEPNO models, respectively.

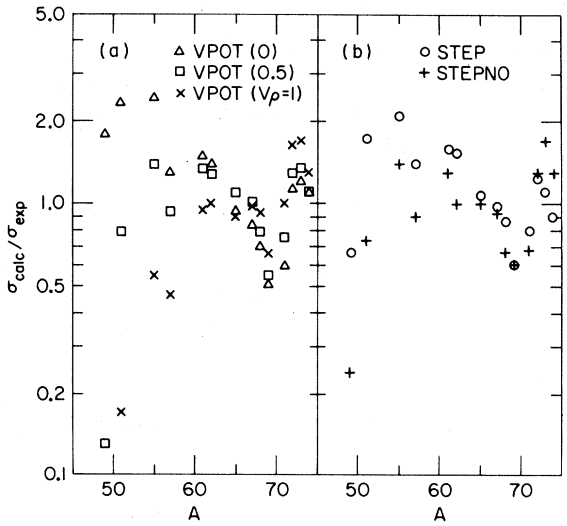

FIG. 9. The ratios of the calculated to experimental cross sections for the mass-yield curve from the interaction of 378-MeV protons with ^{75}As. In Fig. 9(a) the triangles, squares, and crosses are calculated with the VPOT(0), VPOT(0.5), and VPOT($V\rho = 1$) models, respectively. In Fig. 9(b) the circles and daggers are calculated with the STEP and STEPNO models, respectively.

sults obtained from the above model and the STEP and STEPNO models of Ref. 4. The latter two models refer to the calculations done with the velocity-independent potential. The STEP model included refraction and reflection, while the STEPNO model did not.

III. COMPARISON AMONG MODELS AND EXPERIMENTAL DATA

Three types of experimental data were chosen for comparison with the different model calculations:

(1) excitation functions for spallation reactions,
(2) mass yields in spallation reactions,
(3) energy and angular distributions of emitted "fast" nucleons.

First, the experimental and calculated excitation functions for the production of various nuclides from the interaction of protons with ^{209}Bi will be compared. Figures 1–6 show the excitation functions for the $(p, 8n)$, $(p, 9n)$, $(p, p7n)$, $(p, p3n)$, $(p, 2p6n)$, and $(p, 2p5n)$ reactions[9] from ^{209}Bi, respectively. These particular excitation functions were chosen to give two examples each of (p, xn), (p, pxn), and $(p, 2pxn)$ reactions: one showing very good agreement between calculation and experiment and the other showing not such good agreement. In all cases except the ^{209}Bi-$(p, 2p5n)^{203}$Pb excitation function, the VPOT($d \neq 0$) models give better agreement with experiment than the STEP model. Further, in all cases except the ^{209}Bi$(p, 2p5n)^{203}$Pb excitation function the results from the VPOT($V\rho = 1$) model either agree with experiment better than the STEPNO results or are statistically the same as these latter results. The immediate conclusion that one can draw from these comparisons is that even an ap-

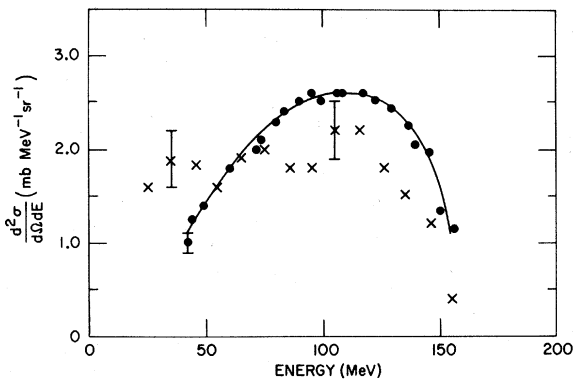

FIG. 10. Differential cross section for protons emitted at 30° in the laboratory system in the interaction of 160-MeV protons with ^{209}Bi. The solid circles are the experimental data of Ref. 15 and the crosses were obtained from the VPOT($V\rho = 1$) calculation.

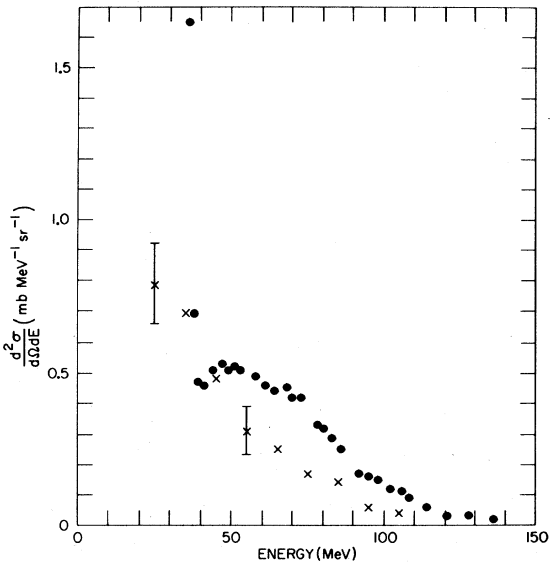

FIG. 11. Differential cross section for protons emitted at 80° in the laboratory system in the interaction of 160-MeV protons with ^{209}Bi. Symbols have same meaning as in Fig. 10.

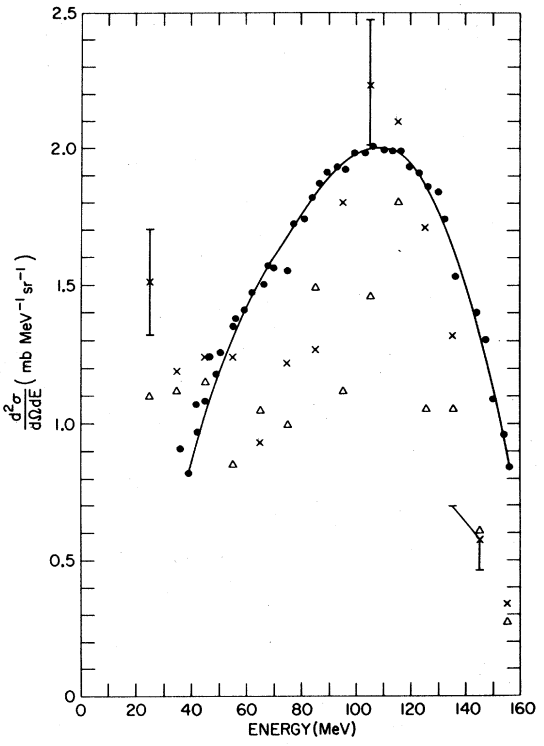

FIG. 12. Differential cross section for protons emitted at 30° in the laboratory system in the interaction of 160-MeV protons on ^{58}Ni. The solid circles are the experimental data of Ref. 15. The triangles and crosses were obtained from the VPOT(0) and VPOT($V\rho = 1$) calculations, respectively.

proximate inclusion of short-range nucleon correlations in intranuclear-cascade calculations of excitation functions for rather complex reactions generally improves the agreement with experiment, without sacrificing the classical refraction and reflection of the cascade nucleons.

In Figs. 7 and 8 the excitation functions for two (p,pn) reactions are presented. In Fig. 7 there is shown a comparison between calculated[10] and experimental excitation functions[11] for ^{197}Au-$(p,pn)^{196}$Au. The VPOT($d \neq 0$) results agree better with experiment than the STEP results, and the VPOT($V\rho = 1$) results are statistically the same as the STEPNO results. Neither of these conclusions can readily be drawn from the experimental[12] and calculated excitation functions for the ^{65}Cu(p,pn)-^{64}Cu reaction shown in Fig. 8. In this case the STEPNO results agree slightly better with experiment than the VPOT($V\rho = 1$) results.

Comparisons between experimental and calculated excitation functions do not always indicate the differences between various intranuclear-cascade models because some calculated cross sections are extremely dependent on the evaporation calculations that follow the intranuclear cascades. This is especially true when large numbers of particles are evaporated. For this reason a second type of comparison between observed and calculated cross sections is made: a comparison between calculated and experimental mass yields. In such comparisons the dependence of calculated cross sections on evaporation details is somewhat diminished because in the evaporation calculation the yield of a given mass does not depend too strongly on the branching ratio for the emission of a proton or a neutron, since both processes lead to the same mass.

Accordingly, in Figs. 9(a) and 9(b) a comparison of the ratios of the calculated-to-experimental cross sections for the production of various masses from the interaction of 378-MeV protons with ^{75}As is given. The experimental data are those of Cumming[13] and extend over almost 3 orders of magnitude with values of ~100 mb for $A = 74$ and ~0.5 mb for $A = 50$. Hence, the comparisons near $A = 50$ may not be very meaningful. If one uses $\sum_A |(\sigma_{\text{calc}}/\sigma_{\text{exp}})_A - 1|$ as the measure of the over-all agreement between calculated and experimental mass yields, then the VPOT(0.5) and STEPNO mass yields agree slightly better with the experimental mass yields than those obtained from the other three models.

In all the excitation-function and mass-yield calculations, the evaporation phase of the reaction was calculated by the method described by Dostrovsky, Fraenkel, and Friedlander[14] and without any parameter variations.

A third type of experimental data, and one that can be directly compared with the output from intranuclear-cascade calculations, is the energy and angular distributions of emitted "fast" protons. Figures 10 and 11 present experimental[15] and calculated spectra of protons emitted at 30 and 80°, respectively, from the interaction of 160-MeV protons with ^{209}Bi. The VPOT($V\rho = 1$) model reproduces the experimental spectra as well as does the STEPNO model and better than the STEP model (refer to Figs. 8 and 9 of Ref. 4 for the STEP and STEPNO results). In Fig. 12 the calculated and observed[15] spectra of protons emitted at 30° from the interaction of 160-MeV protons with ^{58}Ni are presented (refer to Fig. 11 of Ref. 4 for the STEP and STEPNO results). None of the calculated spectra reproduce the experimental spectrum very well. However, both VPOT models do a better job than the STEP model, and the VPOT($V\rho = 1$) model reproduces the experimental spectrum about as well as the STEPNO model does.

IV. SUMMARY

The effect of including short-range nucleon correlations in an approximate manner in intranuclear-cascade calculations using a velocity-dependent potential has been studied. In these calculations the refraction and reflection of cascade nucleons were treated classically. It was found that the inclusion of these correlations leads, in general, to better agreement with a variety of experimental data. Further, the agreement with experiment in most cases was as good as or better than that obtained from the STEPNO model. It is rather difficult to explain why the STEPNO model, which neglects both the refraction and reflection of cascade nucleons as well as nucleon correlations, reproduces experimental data so well. However, it is possible that the neglect of short-range correlations, through rather fortuitous cancellation of effects, makes up for the neglect of reflection and refraction in the STEPNO model. In any case, it is satisfying to have found a physically more reasonable model than STEPNO that gives fair agreement with experimental results.

---

*Research performed under the auspices of the U. S. Atomic Energy Commission.

[1]M. L. Goldberger, Phys. Rev. 74, 1269 (1948).
[2]N. Metropolis, R. Bivins, M. Storm, A. Turkevich, J. M. Miller, and G. Friedlander, Phys. Rev. 110, 185 (1958); 110, 204 (1958).
[3]H. W. Bertini, Phys. Rev. 131, 1801 (1963).
[4]K. Chen, Z. Fraenkel, G. Friedlander, J. R. Grover,

J. M. Miller, and Y. Shimamoto, Phys. Rev. 166, 949 (1968).
[5]K. Chen, G. Friedlander, and J. M. Miller, Phys. Rev. 176, 1208 (1968).
[6]*Thermal Neutron Scattering*, edited by P. A. Egelstaff (Academic, New York, 1965).
[7]E. J. Moniz, G. D. Nixon, and J. D. Walecka, in *High Energy Physics and Nuclear Structure*, edited by S. Devons (Plenum, New York, 1970).
[8]R. Hofstadter, Ann. Rev. Nucl. Sci. 7, 295 (1957).
[9]Y. Le Beyec and M. Lefort, Nucl. Phys. A99, 131 (1967); R. Bimbot and M. Lefort, J. Physique 27, 385 (1966).
[10]The calculation was actually for ^{209}Bi$(p,pn)^{208}$Bi, which is expected to be indistinguishable from that for ^{197}Au$(p,pn)^{196}$Au.
[11]H. P. Yule and A. Turkevich, Phys. Rev. 118, 1591 (1960).
[12]A. A. Caretto, U. S. Atomic Energy Commission Report No. NYO-10693, 1964 (unpublished).
[13]J. B. Cumming, Ph.D. thesis, Columbia University, New York, 1954 (unpublished); and private communication.
[14]I. Dostrovsky, Z. Fraenkel, and G. Friedlander, Phys. Rev. 116, 683 (1959).
[15]P. G. Roos, Ph.D. thesis, University of Maryland, College Park, 1964 (unpublished); and private communication from S. Wall.

PHYSICAL REVIEW C VOLUME 4, NUMBER 6 DECEMBER 1971

Resolution of Fixed-Geometry Optical-Model Ambiguities*

B. D. Watson,† D. Robson,‡ D. D. Tolbert,§ and R. H. Davis
Department of Physics, The Florida State University, Tallahassee, Florida 32306
(Received 27 August 1971)

In order to test a procedure for resolving the problem of discrete real-well-depth ambiguities found in optical-model analyses, α particles were elastically scattered from ^{70}Ge, ^{90}Zr, ^{107}Ag, and ^{140}Ce at incident energies from 0.6 to 1.2 times the classical Coulomb-barrier height for each nucleus. The real and imaginary nuclear potential-well radii and the Coulomb radius (assuming a uniformly charged sphere) for each nucleus were taken to be $R=R_C=r_0(A_{\text{Alpha}}^{1/3}+A_{\text{Target}}^{1/3})$, where $r_0=1.22$ F. A diffuseness of 0.57 F was used throughout. For three of the nuclei, only one pair of real (U) and volume-imaginary (W) potentials was found, with the real-well depth for ^{90}Zr showing a slight energy dependence. The potentials obtained were (in MeV): $U=23.5$, $W=11.0$ for ^{70}Ge; $U\sim22$, $W\sim10.3$ for ^{90}Zr; $U=25.5$, $W=14.5$ for ^{107}Ag; and $U=18.0$, $W=6.0$ for ^{140}Ce. Analysis of angular distributions taken with 15–18-MeV α particles did not yield evidence of expected ambiguities in the real-well depth, so further calculations were performed in which the effect of absorption was more generally explored. The usefulness of the proposed method was found to be limited to cases where the absorption is either ineffective, or small compared with the average spacing between single-particle levels of the same spin and parity.

I. INTRODUCTION

It is well known that optical-model analyses of elastic scattering data using the Woods-Saxon potential form factor have been unable to experimentally distinguish between several values for the real potential well depth, because nearly equivalent cross sections were predicted for each. Two types of ambiguity have been observed. Examples of the first type[1-3] were derived from analyses in which only the optical-potential strengths were variable while the Woods-Saxon geometrical form factors were held constant. A series of solutions is found for the real-potential strength, extending from about 20 to about 200 MeV and spaced by roughly 30 MeV. Potentials which are ambiguous in this discrete manner are hereinafter called type-one potentials. Previously, type-one ambiguities have been found with some certainty in the analyses of α-particle scattering from ^{24}Mg, ^{32}S, and ^{40}Ca.

Ambiguities of the second type differ from those of the first in that all parameters are free and several different real-well depths may be obtained, but only if compensating changes are made in the geometrical parameters so that the Woods-Saxon potential tails of the different optical-parameter sets effectively appear to be of nearly equivalent strength, and indeed may all converge at the "strong-absorption" radius R_{SA}.[4] The strong-absorption radius is analogous to the classical turning point for a particle with angular momentum l. In quantal terms, this radius is defined by $kR_{SA}=\eta+[\eta^2+l(l+1)]^{1/2}$. Here η is Coulomb parameter and l is the angular momentum for which $\mathrm{Re}(S_l)=\frac{1}{2}$, where S_l is the S matrix element for partial wave l. Type-two ambiguities have also been